

# Influence of microwaves in the early stage of alkali activation on the mechanical strength of alkali-activated materials

Barbara Horvat<sup>\*</sup>, Majda Pavlin, Vilma Ducman

Slovenian National Building and Civil Engineering Institute, Dimičeva ulica 2, 1000, Ljubljana, Slovenia

## ARTICLE INFO

### Keywords:

Waste material  
Alkali activation  
Microwave irradiation  
Mechanical strength

## ABSTRACT

This study focuses on the influence of microwave irradiation dosimetry on alkali-activated slurry in its early stages. The impact on the chemistry and mineralogy along with the mechanical properties were evaluated by changing the power of microwaves and their duration of exposure. This influenced the dissolution of amorphous content, diffusion, and self-assembly into an aluminosilicate network. The precursors used in this study were metakaolin, a non-waste material commonly used in geopolymerisation technology, and local fly ash and ladle furnace slag as secondary materials. Furthermore, they were chemically and mineralogically analysed, and their mixtures with NaOH and Na-water glass provided the optimal ratio of the amount of elements obtained using the pre-calculation approach. However, the potential extra addition of water was experimentally determined to allow complete wetting of the material and solid workability during moulding. Using Fourier-transform infrared spectroscopy, the influence of water was further investigated in alkali-activated slag and fly ash irradiated with microwaves, which resulted in the highest values of mechanical strength in the dosimetry-mapping part of the analysis. In addition to the time dependence of the expected mechanical strength on the ageing of the alkali-activated material, the synthesised material exhibited a significant dependence on the dose of microwave irradiation, which was different for every precursor as well as every mixture with different chemistries.

## 1. Introduction

Alkali-activated materials (AAMs) are considered promising alternatives to conventional building materials (cement, concrete, and ceramics) because of the reduced energy requirements for AAM production, that is, the preparation time and temperature are low, resulting in a low carbon footprint [1,2]. Materials being used as precursors must contain a sufficient amount of Si and Al in the amorphous content and as few elements of the first group of the periodic system as possible, which are added later with the alkali activator considering the final ideal molar ratio of the amount of elements M:Al:Si (M is the elements of first group) of all the ingredients together is 1:1:1.9 [3].

The most used precursor is metakaolin, which is considered the standard in alkali activation [4]. However, the most used alkalis in alkali-activators are NaOH, KOH, Na-water glass, and K-water glass.

In the first phase of the reaction in an alkaline medium, dissolution of the precursor occurs, followed by the transport of the elements, aluminosilicate monomer formation (binding of Al and Si with O into tetrahedra), and finally, polycondensation (and dehydration) into the

aluminosilicate network, which is mostly amorphous [5].

Curing is performed either at room temperature or in drying chambers, where heating is superficial [6] and takes a certain amount of time to reach the inner parts of the moulded alkali-activated slurry even if the heating chamber is at the desired temperature at the beginning of curing. Conversely, implementing (dielectric) heat with microwave irradiation is volumetric [6] only if the material's electrical and magnetic properties classify it as an absorbent, that is, the material absorbs microwaves and exchanges electromagnetic energy. Other types are classified as transparent materials (insulators), where microwaves travel through the material without energy transfer, and opaque materials, where microwaves fully reflect on their surface without energy transfer. Real-life materials (waste materials) usually comprise different phases that interact with microwaves selectively, that is, some phases absorb microwave energy, some reflect microwaves, and some are invisible to them [7]. Molecules with permanent dipole moments "interact" with microwaves well [8], i.e., there is at least one component in the mixture that will be efficiently irradiated (water). This mixed absorption results in the material being heated non-uniformly throughout the material's

<sup>\*</sup> Corresponding author.

E-mail address: [barbara.horvat@zag.si](mailto:barbara.horvat@zag.si) (B. Horvat).

<https://doi.org/10.1016/j.ceramint.2022.12.133>

Received 15 October 2022; Received in revised form 13 December 2022; Accepted 13 December 2022

Available online 14 December 2022

0272-8842/© 2023 The Authors. Published by Elsevier Ltd. This is an open access article under the CC BY-NC-ND license (<http://creativecommons.org/licenses/by-nc-nd/4.0/>).

volume, which can be solved with a microwave oven that generates microwaves of variable frequencies simultaneously [9]. Additionally, the frequency spectra of kitchen microwave ovens are not monochromatic (considering microwaves can interfere with neighbouring frequencies, it was chosen that kitchen microwave ovens operate at approximately 2.45 GHz whereas industrial microwaves operate at approximately 0.915 GHz with few MHz of space of “not-used” frequencies) and range from 2.40 to 2.50 GHz with several broader peaks [10].

In recent years, only a few articles have studied the influence of microwave heating on AAMs.

- Microwave heating of alkali-activated coal bottom ash allowed AAM to develop its microstructure faster, and the mechanical properties were enhanced in a short time; however, if microwave heating was conducted for too long, the structure deteriorated and the strength decreased [11]. The alkali-activated slurry was cured at 75 °C for 48 h and then irradiated in a microwave oven at 700 W.
- Already demoulded alkali-activated coal bottom ash that had been cured at low temperatures for less than 36 h was irradiated in a microwave oven for 3 min, which rapidly increased its compressive strength [12].
- Alkali-activated coal bottom ash was pre-dry-oven cured for 12/24/36 h at 75 °C, and post-microwave oven heated for up to 7 min at 700 W. The specimens cured for 36 h showed a high improvement in compressive strength just after being irradiated with microwaves for 3 min (from 13 MPa to 40 MPa) [13].
- Alkali-activated coal bottom ash was pre-cured in a dry oven at 75 °C and irradiated with microwaves of different power for different durations. It was noticed that the compressive strength depended on the moisture content, i.e., the highest compressive strength was achieved if the moisture was between 4 and 6% (average surface temperature between 120 and 130 °C). If lowered with further microwave irradiation, the compressive strength decreased owing to the loss of chemically bonded water (internal stress became high) in the AAM. A higher compressive strength was achieved after 1 d of conventional curing followed by short microwave irradiation compared to when the samples were cured at 75 °C for 7 and 21 d [14].
- Malaysian researchers investigated the influence of microwave curing of samples cured from 60 °C to 120 °C for 24 h, demoulded, and cured further at 60 °C for 48 h in a steam oven after 1 h at room temperature, or with microwave heating from 20 to 140 min. The density of samples prepared with microwave heating was higher than that of samples prepared with surface heating for all mixtures. The compressive strength increased as the temperature increased when conventional heating was used, and with time under microwave irradiation. The highest compressive strength was achieved using microwave heating [15].
- Alkali-activated mortar from pond fly ash containing heavy metals was prepared at 80 °C for 4, 8, and 12 h, and with microwave heating for 10–60 min in steps of 10 min. It was observed that 60 min of microwave irradiation resulted in a much higher compressive strength than that of the samples cured at 80 °C for 12 h. Furthermore, the choice of proper alkali and alkali glass is important [16].
- High-strength alkali-activated fly ash was obtained with microwave irradiation in a shorter time compared to samples prepared by surface heating. Specimens were demoulded after 24 h and then treated in ambient air (23 °C and 50% humidity) and water (23 °C). The samples that were not demoulded were treated in a conventional oven for 1–2 h at 60 °C and 90 °C, whereas the demoulded samples were treated at 90 °C and 120 °C, or in a microwave oven for 5–105 min. The result showed that if the curing temperature was higher, higher compressive strength was achieved faster, the influence of dehydration had a minor effect on strength development, and the compressive strength increased with time at high temperatures. This confirmed that the temperature of the samples depended on the

microwave power and time under microwaves, that is, the higher the power and longer the time, the higher the temperature of the sample. The highest compressive strength with microwave irradiation for 15 min was achieved with microwaves of 300 W; no cracks were observed at 200 W, whereas higher microwave powers resulted in specimen deterioration and a decrease in mechanical strength. The compressive strength increased with the microwave curing time (curing at 200 W). The mechanical strengths of the samples prepared by microwave heating were higher than those of the samples cured at 90 °C. It was also observed that the compressive strength of smaller samples is higher at shorter curing times than that of larger samples considering the temperature of the core of the smaller sample evolved faster at a higher temperature, that is, microwaves were absorbed in the material and reach a certain depth (depending on their power), while surface heating required significantly more amount of time to reach the core. It was concluded that AAMs with high strength can be achieved in a short time by controlling the microwave power, temperature, and specimen size [17].

- Porous alkali-activated fly ash-based material was synthesised by microwave irradiation of the slurry for 1 min after mixing all reagents for 1 min, where the microwave power was the only variable [18].
- Precursor rice husk ash was incinerated by microwave heating and used with fly ash for alkali-activated (geopolymer) concrete; however, there was no comparison with the use of non-microwave-incinerated rice husk ash [19].
- In addition to the treatment of precursors and AAMs, microwave technology was used for synthesising silica fume-based solid activators for fly ash geopolymerisation, one part precursor by dehydration of used-prepared alkalis varying the kitchen microwave oven's power and irradiation time [20].

In this study, microwaves of different powers and durations were used on moulded slurries of alkali-activated metakaolin, ladle furnace slag, and fly ash to influence the early stages of alkali activation. After microwave irradiation material was cured at room temperature and 55% moisture (the majority of other studies did not use microwave irradiation instantly and cured their materials first using conventional methods). The results were compared with their not irradiated counterparts cured solely at room temperature and 55% moisture. Alkali-activated slag and fly ash was further prepared with different amounts of water and irradiated with microwaves of power and duration that resulted in the highest compressive strength for each material.

## 2. Materials and methods

### 2.1. Characterisation of precursors and their alkali-activated counterparts

Fly ash (FA), ladle furnace slag (SR), and metakaolin (MK) were dried (70 °C for 24 h in a heating chamber WTB Binder), ground (with a vibrating disk mill Siebtechnik), and sieved below 125 µm for X-ray powder diffraction (XRD) and X-ray fluorescence (XRF) analysis.

The XRD (Empyrean PANalytical X-ray Diffractometer, Cu X-ray source) pattern was obtained using X'Pert Highscore plus 4.1. The amount of amorphous content and minerals was estimated by Rietveld refinement using an external standard (pure corundum, Al<sub>2</sub>O<sub>3</sub>).

For XRF, the dried precursors were first ignited at 550 °C (removal of organic material), then at 950 °C (removal of carbonates), and then melted into discs (the precursor was mixed with Fluxana<sub>(s)</sub> FX-X50-2, that is, a mixture of lithium tetraborate and lithium metaborate (mass ratio 1:1), to lower the melting point, in a mass ratio of 1:10 for Fluxana; LiBr<sub>(l)</sub> (prepared from 50 ml H<sub>2</sub>O and 7.5 g of LiBr<sub>(s)</sub> from Acros Organics) was added to the mixture of precursor and fluxana to avoid glueing the melt onto the platinum vessel). XRF was performed on discs (Thermo Scientific ARL Perform'X Sequential XRF) from fluorine to americium, and the measured data were analysed using UniQuant 5.

The bending and compressive strengths of the AAMs were measured using a compressive and bending strength testing machine (ToniTechnik ToniNORM) at 7, 14, 21, and 28 d after moulding. Experiments with additional water were performed on 1, 3, and 7 d. The age of the sample when its mechanical strength was measured was denoted as *t*.

Fourier-transform infrared spectroscopy (FTIR; PerkinElmer Spectrum Two) was performed in ATR mode on samples with additional water after mechanical strength measurements.

The geometrical densities of the alkali-activated materials were determined by weighing the alkali-activated prisms and dividing their mass by their volume.

## 2.2. Preparation of precursors and their characterisation results used for determination of mixture designs of alkali-activated samples activated by Na-based alkalis

The FA and MK precursors were used as received without further treatment. On the other hand, SR was ground (with the vibrating disk mill Siebtechnik) and sieved below 125  $\mu\text{m}$ . Their true densities were determined with a pycnometer according to SIST EN 1097–7:2008 using petroleum (density of FA, SR and MK are 2.4  $\text{kg}/\text{dm}^3$ , 2.8  $\text{kg}/\text{dm}^3$ , and 2.5  $\text{kg}/\text{dm}^3$  respectively).

From the XRF and XRD results of all precursors, the amount of amorphous content was determined for each chemical element according to our previous work [21] and is presented in Table 1. The loss on ignition (LOI) was measured at 550  $^{\circ}\text{C}$  and 950  $^{\circ}\text{C}$ .

The required addition of alkalis (NaOH (Donau Chemie Ätznatron Schuppen, EINECS 215-785-5, Vienna, Austria) and Na-water glass (Geosil, 344/7, Woelner, Ludwigshafen, Germany, with a mass percentage of  $\text{Na}_2\text{O}$  16.9%, and mass percentage of  $\text{SiO}_2$  27.5%)) was calculated to achieve the molar amount of elements M:Al:Si of all ingredients together 1:1:1.9. First, the amount of Si was fixed at an Al: Si ratio of 1:1.9 to achieve the highest compressive strength [3]. Then, the first group of the periodic system was considered to avoid efflorescence, that is, keeping the ratio  $\text{M}:\text{Al} \leq 1$ . Furthermore, it was taken into account, that elements from the second group of the periodic system did not participate in the reaction (“a” black rows in Table 2); however, in case they do get involved in the reaction, the addition of NaOH was eliminated. This was possible only in the case of FA (mixture “FAB” in Table 2), considering optimal mixtures from MK and SR had enough elements from the first group of the periodic system owing to the addition of Na-water glass while fixing the ratio  $\text{Al}:\text{Si} = 1:1.9$  (as presented in Table 3). For all chemically optimal mixtures (FAa, SRa, MKa) that needed extra liquid to gain solid workability (sufficient wetting of the pulverised material and easy enough moulding of the slurry), a minimal amount of distilled water was added (determined by trial and error). The added distilled water was replaced by Na-water glass (the mass of the liquid was kept constant) only as a room temperature early “liquid” reference (no microwave irradiation), grey rows in Table 2; FAc, SRb, MKb. The goal of this experiment was to increase the viscosity of the slurry to increase the final compressive strength (slurries with higher

**Table 1**

The LOIs and mass percentage of elements from fluorine to americium (measured with XRF, 1st row), of elements in the crystalline phase (determined with Rietveld refinement from XRD, 2nd row), and of elements in the amorphous content (3rd row).

Precursor	Elements [m%]	Na	K	Cs	Mg	Ca	Sr	Ba	Al	Si	LOI 550 $^{\circ}\text{C}$	LOI 950 $^{\circ}\text{C}$
FA	XRF	0.89	1.83	0	1.69	8.85	0.05	0.07	12.16	20.92	0.85	0.89
	XRD	0	0	0	0.37	1.64	0	0	1.74	4.32		
	XRF-XRD	0.89	1.83	0	1.32	7.21	0.05	0.07	10.42	16.60		
SR	XRF	0.27	0.16	0	17.94	25.48	0.05	0.02	3.53	8.18	4.53	17.40
	XRD	0	0	0	6.97	13.82	0	0.02	0.75	7.41		
	XRF-XRD	0.27	0.16	0	10.97	11.66	0.05	0	2.78	0.77		
MK	XRF	0.21	0.15	0	0.10	0.35	0.005	0.04	13.54	32.41	1.36	2.03
	XRD	0	0	0	0	0	0	0	1.58	16.20		
	XRF-XRD	0.21	0.15	0	0.10	0.35	0.005	0.04	11.96	16.21		

**Table 2**

AAM mixtures prepared from FA, SR and MK: optimal mixtures FAa, SRa, and MKa, mixture with the inclusion of the second group influence from the precursor and the exclusion of additional Na from alkali (FAB), “liquid” reference mixtures (FAc, SRb, MKb, grey rows). The mixtures with additional amounts of water content (FAd, FAe, SRc, SRd, blue rows). The amount of water content is fully deducted from water added to the mixture ( $m_{\text{H}_2\text{O}}$ ), whole water present in the mixture ( $m_{\text{H}_2\text{O whole}}$ ) and its mass percentage in the slurry ( $m\%_{\text{H}_2\text{O whole}}$ ).

Mixture	$m_{\text{precursor}}$ [g]	$m_{\text{NaOH}}$ [g]	$m_{\text{Na-water glass}}$ [g]	$m_{\text{H}_2\text{O}}$ [g]	$m_{\text{H}_2\text{O whole}}$ [g]	$m\%_{\text{H}_2\text{O whole}}$ [%]
FAa	50	3	15	2.5	10.8	15.4
FAB	50	0	15	2.5	10.8	16.1
FAc	50	0	17.5	0	9.7	14.4
FAd	50	3	15	5	13.3	18.3
FAe	50	3	15	7.5	15.8	21.0
SRa	50	0	18	5	15.0	20.6
SRb	50	0	23	0	12.8	17.5
SRc	50	0	18	10	20	25.7
SRd	50	0	18	15	25	30.1
MKa	50	2.5	28	5	20.6	24.1
MKb	50	0	33	0	18.3	22.1

viscosity liquids usually dry slower, dehydration leaves material less damaged, but the limit value of mechanical strength is reached after a long time) [21]. With mixtures FAa and SRa, the influence of the amount of water on the irradiation of the AAM slurry was tested by adding higher amounts of distilled water (mixtures FAd, FAe, SRb, SRc; blue rows in Table 2). All prepared mixtures in mass ratios are presented in Table 2 with the total amount of water ( $m_{\text{H}_2\text{O whole}}$ ), which is the added amount of distilled water ( $m_{\text{H}_2\text{O}}$ ) and water present in Na-water glass, and with the mass percentage of water ( $m\%_{\text{H}_2\text{O whole}}$ ), which is calculated on the mass of all ingredients.

In alkali-activated reactions, useful chemical elements in precursors are elements from the first group of the periodic system (Li, Na, K, Rb, Cs), second group (Be, Mg, Ca, Sr, Ba), and as the main building blocks Si and Al, connected with/through oxygen in the aluminosilicate network (ASN) [5]. These elements have to be part of the amorphous content to dissolve in alkali media (Table 1) [5,21] and be well pulverised for the liquid to have access to the inner parts of the powders [22]. In addition to the precursor elements participating in ASN formation, building blocks also come from alkalis (Si from water glasses, first and second group elements from alkalis). The sum of the amorphous elements (from precursors and used alkalis) potentially available for ASN formation in AAM mixtures are presented in Table 3 as molar ratios normalized to Al. “Usefulness” of precursors regarding alkali activation is presented also in Table 2 as mass percentages of the sum of elements that can contribute to ASN, once with and once without the second group (if amorphous elements from the second group dissolve completely, or do not dissolve at all), but always dissolve with oxygen included (but only the amount needed for Al and Si in the ASN). The theoretical differences in the amounts of ASN between mixtures of the same precursor can vary only owing to the slightly different amounts of alkali (Si and Na atoms), which was neglected in the first approximation.

**Table 3**

Molar amount of the elements useful in alkali activation normalized to Al for AAM mixtures and mass percentage of useful elements with ( $m_{\% \text{ US}}$ ) and without ( $m_{\% \text{ US}/2\text{nd}}$ ) the second group present only in precursors (oxygen included).

Mixture	First group [mol]	Second group [mol]	Al [mol]	Si [mol]	$m_{\% \text{ US}}$ [%]	$m_{\% \text{ US}/2\text{nd}}$ [%]
FaA/ FAd/ FAe	1.03	0.61	1	1.89	70.0	61.0
FAb	0.64	0.61	1	1.89		
FAc	0.71	0.61	1	1.95		
SRa/ SRc/ SRd	2.06	7.21	1	1.87	30.8	8.2
SRb	2.59	7.21	1	2.31		
MKa	1	0.03	1	1.89	61.8	61.3
MKb	0.84	0.03	1	1.99		

Slurry mixtures were placed into silicon moulds of size  $(80 \times 20 \times 20) \text{ mm}^3$  and cured at room temperature with 55% moisture (no irradiation; all mixtures), or immediately irradiated in a microwave oven (Gorenje Microwave oven MO 17DV, Slovenia, Velenje, maximal power 700 W, frequency 2.45 GHz) with microwaves with power ( $P_{\text{microwaves}}$ ) from 20%, 40%, 60%, 80%, and 100% of 700 W for 5 s, 10 s, 15 s, 20 s, 25 s ( $t_{\text{microwaves}}$ ; mixtures FAa, FAb, SRa, MKa). Then, it was cured at room temperature and 55% moisture to determine mechanical strength dependence on the irradiation dose. The theoretical energy emitted from the microwave oven to the sample is shown in Fig. 1 (black dots indicate the performed experiments, including the (0,0) point), where we considered that microwaves were present throughout the selected time (starting without any delay) of the irradiation at the chosen power (cyclic operation of the microwave oven was neglected). During each irradiation with microwaves, the entire mould (six prisms filled with the AAM slurry to the top; always only one mould) was positioned centrally in the oven to gain the best possible uniformity of irradiation, and the dose of irradiation was split into all prisms as equal as possible every time.

Mixtures FAa, FAd, FAe, SAa, SRc, SRd were irradiated for 15 s and 20 s at 40% and 60% microwave power before being further cured at room temperature with 55% moisture to determine the influence of the amount of water. All samples were cured (after irradiation) under the same conditions until mechanical strength measurement.

AAMs were demoulded when hardened, that is, SR and MK were demoulded 1 d after moulding their alkali-activated slurries, while FA was demoulded after 3 d.

The bending and compressive strengths, as well as geometrical density contour plots, were calculated with the statistical software JMP 16.0.0, using the Delaunay triangulation of a discrete point set as an algorithm. The points used for the calculation are presented as black dots in Fig. 1 (including point (0,0)).

### 3. Results and discussion

#### 3.1. Analysis of precursor and alkali-activated slurry design

The LOI measured at 550 °C (Table 1) was negligible for MK and FA, whereas, for SR, it was close to 5 m%. This loss can be attributed to water, organic compounds, and/or materials that require less energy to break chemical bonds, such as portlandite [23]. If these materials do not dissolve in alkali, they can dissolve in a high-power curing regime: high temperature, which is not needed when performing conventional temperature curing of AAMs, or energy transfer from the microwaves through the vibration of molecules with permanent dipole moments, that is, from the surrounding water molecules or organic materials themselves. The LOI measured at 950 °C showed that SR contained a significantly higher amount of carbonates than FA and MK. In short periods of irradiation and low microwave powers, the bonds in carbonates most likely cannot be broken, which indicates that carbonates present in the precursor were not available during alkali activation and

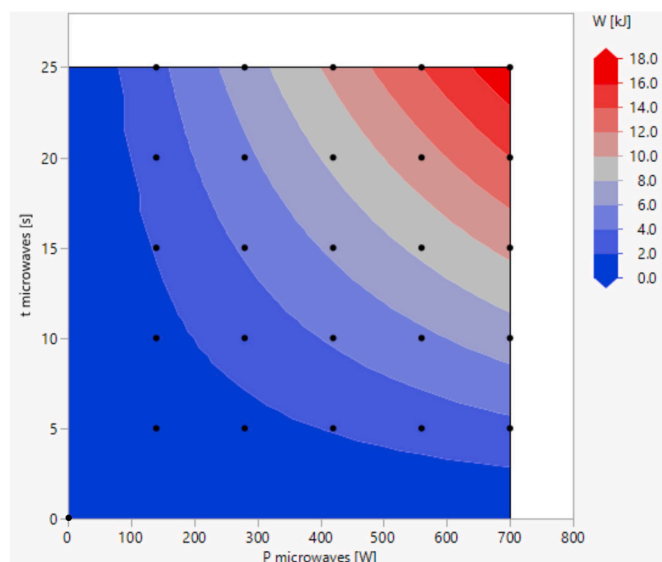


Fig. 1. The energy emitted from the microwave source to the moulded alkali-activated slurry. Black dots label performed experiments.

did not influence the chemistry of the ASN.

The XRF and XRD data of precursors are presented in section 2 (XRD patterns of precursors are presented in the supplement in Fig. S1, Rietveld refinement in the supplement in Fig. S2, labelled peaks in the supplement in Fig. S3) alongside the determination and explanation of mixtures prepared for this study. The highest and lowest amount of water calculated for all ingredients in alkali activation was 30.1% (SRd) and 14.4% (FAc), respectively. A higher amount of water means that more molecules absorb microwaves, but simultaneously, the dose of irradiation is spread to more points in the alkali-activated slurry, heating it more uniformly but slower, and not at the same temperature (the effect of dissolution is therefore lower). The negative effect of an excessive amount of water decreased the penetration depth of the microwaves [24,25], leading to non-uniform heating throughout the volume of the moulded alkali-activated slurry. In addition, too much water can lead to lower compressive strength in AAMs cured in a conventional way [21], making it difficult to distinguish between the positive and negative effect(s) of the different amounts of water.

Mixtures closest to the optimal molar ratio of elements 1:1:1.9 for M: Al:Si is MKa and FAa/FAd/FAe, where MKa has almost no element of the second group in the amorphous content that would participate in the alkali-activated reaction and cause a surplus of elements from the first group added into the mixture with alkalis, which causes efflorescence. To avoid potential efflorescence when FA was used as a precursor, a mixture of FAb was prepared without the addition of NaOH. Conversely, mixtures with SR had too large amounts of elements from the first and second groups, regardless of whether they participated in the alkali-activated reaction.

The mass percentage of all useful elements in the alkali activation present in the precursor was the largest in FA (70%), followed by MK (62%), whereas SR only had 31% of material potentially useful in alkali activation (the rest can be considered only as aggregates if they do not dissolve in alkali media). If the second group is considered, the largest mass percentage of useful elements was in MK and FA (61%); this amount was less than 10% for SR.

#### 3.2. Preliminary analysis of alkali-activated mixtures

The compressive (CS) and bending (BS) strengths of non-irradiated mixtures of FA, SR, and MK measured 7 d after moulding are shown in Fig. 2.

Mechanical strengths are highly dependent on the precursor used,

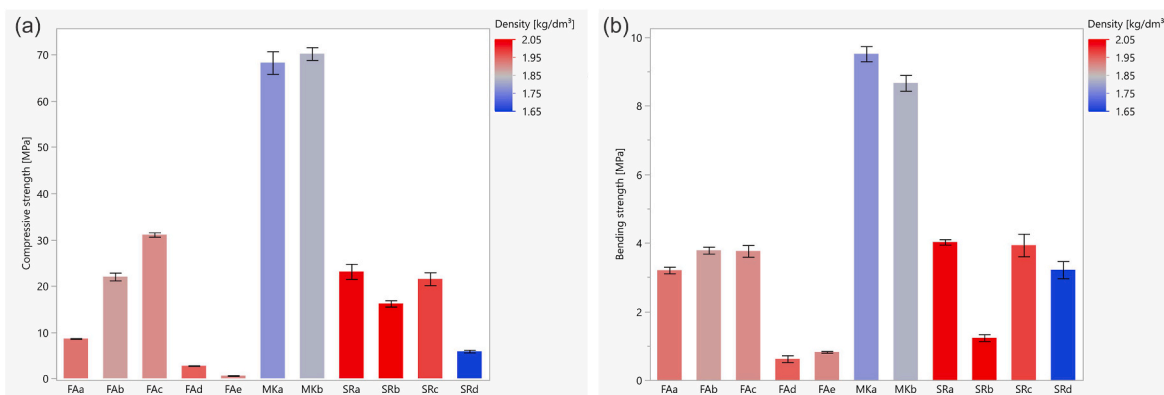


**Fig. 2.** (a) CS and (b) BS coloured according to the geometrical density measured 7 d after moulding of non-irradiated alkali-activated slurries cured solely at room conditions and 55% moisture from all mixtures presented in this paper.

especially on the time needed for hardening of the alkali-activated slurry, that is alkali-activated FA could be demoulded not prior to 3 d after mixing ingredients regardless of the curing procedure used, whereas alkali-activated SR and MK could have been demoulded after a few hours (but were demoulded after 1 d). Previous research [21] shows that AAMs require a certain amount of time to gain final mechanical strength, which indicates that the mechanical strength results after 7 d might not be final for all precursors and their mixtures.

However, from CS of optimal mixtures from different precursors (FAa, SRa, MKa) shown in Fig. 2, it could be falsely concluded that a higher density of AAM indicates lower mechanical strength (alkali-activated MK has a geometrical density of approximately  $1.8 \text{ kg/dm}^3$ , FA  $1.9 \text{ kg/dm}^3$ , and SR  $2.1 \text{ kg/dm}^3$ ), but the higher density of alkali-activated SR comes from a higher density of precursor SR itself (precursor MK has a true density of approximately  $2.5 \text{ kg/dm}^3$ , FA  $2.4 \text{ kg/dm}^3$ , and SR  $2.8 \text{ kg/dm}^3$ ) that also has the smallest amount of alkali-activated reaction useful elements (see Table 3), the lowest mass percentage of amorphous Al and Si, and the highest percentage of amorphous elements from the second group (see Table 1) that might play a role in the alkali-activated reaction; therefore the lower values of compressive strength of SR compared to FA and MK. However, besides geometrical density, which is connected mainly to the porosity (higher porosity, lower geometrical density, usually means lower mechanical strengths [21]) and not just to the precursor used, it is important to determine which material does not react, how it is distributed and connected with ASN, and how it contributes to the skeletal density. A dependence on the change in the amount of Na along with water on the CS was noticed for all precursors used in this study (observations from Fig. 2, Table 2, and Table 3):

- FAa, the initial mixture (the assumption was that amorphous elements from the second group, which are present in the precursor, do not react in alkali activation) has a lower 7 d old CS value compared to mixture FAb, which has a low amount of added Na but a high amount of water (leading to the conclusion that dissolution was slightly lower owing to the water/binder ratio or/and that elements from the second group from the precursor do react at least to a certain degree in alkali media, and that FAa might show efflorescence). Decreasing the amount of water led to an even higher 7 d old CS, that is, FAc had a higher CS than FAb.
- MKa as the initial mixture showed a slightly lower CS compared to MKb, which has a slightly lower amount of Na and water, which is in agreement with our previous work (less water, better CS [21]). A slightly less Na than the theoretically determined from XRF and XRD can also be beneficial if not all Al in the amorphous content dissolves (to avoid efflorescence).

- SRa as the initial mixture shows a higher CS compared to SRb which has a higher amount of Na and a lower amount of water, thereby indicating that the amount of Na is exceeded in the case of SRb (if the same assumption as for FAa for the second group is also valid for SRa; else, the amount of Na also exceeds in mixture SRa).

As shown in Fig. 2, a higher amount of water decreases the mechanical strength: FAe has lower mechanical strengths than FAd, which has lower mechanical strengths than FAa (the amount of water increases in the mixtures). The same conclusion can be drawn from the SR mixtures, that is, SRd has lower mechanical strengths compared to SRc mixtures, which have lower mechanical strengths compared to SRa mixtures, where the amount of water decreases.

### 3.3. Preliminary analysis of irradiation of alkali-activated samples

CS and BS along with the density of alkali-activated mixture FAa (1st row), FAb (2nd row), SRa (3rd row), and MKa (4th row) irradiated with microwaves of different powers and durations, 28 d after moulding, as shown in Fig. 3(a–c), respectively.

The absorbed dose of irradiation depends on the duration and power of the microwaves and the properties of the material that allow (or not) “interaction” with the microwaves. The mass of the irradiated material was approximately constant for each individual mixture (all prisms in the mould were filled equally) but differed slightly among mixtures (different amounts of solid and liquid parts) and precursors (their densities were different). Additionally, the position of the mould in the microwave was always centred so that the only influence on the final properties of the alkali-activated material would be from the used precursor and alkali liquid part of the mixture.

The contour plots of mixture FAa in Fig. 3 (1st row) show that the absorbed dose of irradiation has a unique impact on the mixture FAa. CS, BS, and density without irradiation (point (0,0) on the 2-dimensional plots) were lower than their maximal average value that was reached with irradiation.

If the absorbed dose is too high, the slurry inside starts to deteriorate and the AAM cracks [13]; the deterioration is visible when AAM is ready for demoulding (when it is hardened enough) and not in the slurry. These large-scale cracks severely influence the bending strength; that is, AAM cannot withstand higher dosages of microwaves that influences the rate of dehydration. Changes in the density range from  $1.8$  to  $2.1 \text{ kg/dm}^3$  and show peaks at different levels of emitted microwave energy that indicate different phenomena taking place in the alkali-activated slurry. Optimal values for irradiation with microwaves in a used microwave oven with filled mould and FAa slurry, according to all three plots in Fig. 3, is 40% (280 W) of full microwave power for 15 s, i.e., the energy emitted to the material is 4.2 kJ.

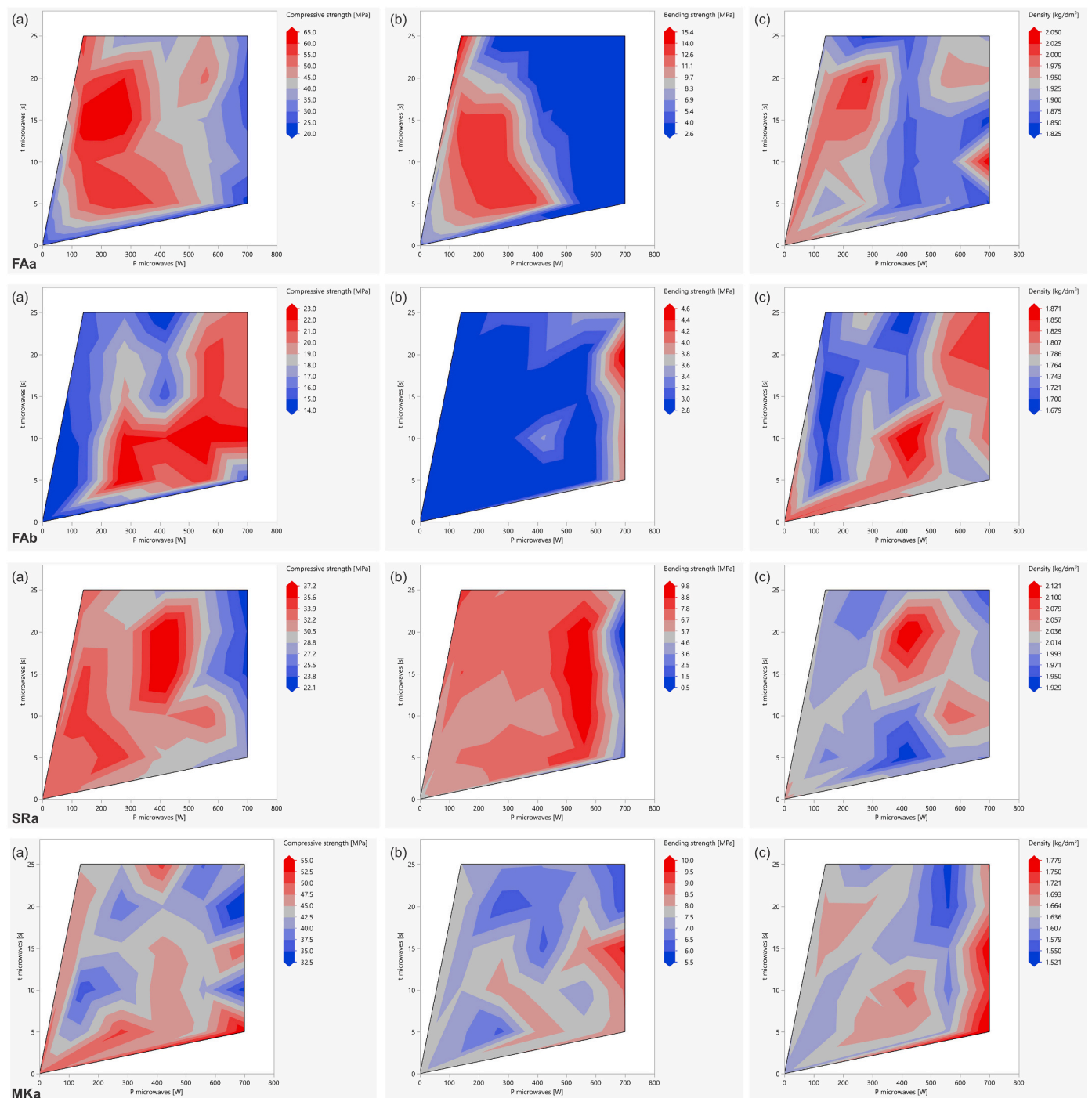


**Fig. 3.** (A) CS, (b) BS, and (c) density of 28 d old alkali-activated mixture FAa, FAB, SRa and MKa showing unique dosimetric dependence on duration and power of irradiation with microwaves.

From Figs. 3 and 1, it can be concluded that other than the amount of absorbed dosage, the time the dosage is absorbed is also important, which can be attributed to the rise in the temperature inside the slurry during microwave irradiation (although not measured, our experimental concludes that not all materials can withstand irradiation of AAM, i.e., the temperature of AAM irradiated with 700 W microwaves for a long time can raise its temperature to “sintering” temperature or above – randomly distributed glowing lines on AAM’s surface were seen) and potential water evaporation that changes its mass percentage in the slurry leading to its potential deficit needed in the reaction.

CS, BS, and the density of the alkali-activated mixture FAB (which is

like FAa without NaOH, ending with a slightly higher mass percentage of water, both leading to lowering pH) irradiated with microwaves of different powers and durations, 28 d after moulding, as shown in the second row of Fig. 3(a–c), respectively.

From the contour plots for mixture FAB it is clear that the influence of microwaves is different for mixtures FAa and FAB, showing peaks of higher density, CS, and BS at 420 W and 10 s of microwave irradiation. After 28 d, the CS and BS of the mixture FAa ended with much higher values than the CS and BS of the mixture FAB, which could be due to the slightly larger amount of initial overall water in the mixture FAB (Table 2), and/or due to the more optimal mixture regarding amounts of

alkali elements and Al (Table 3).

Densification (pre-sintering) of irradiated FAb might start increasing above a microwave power of 700 W (an increase in BS), which is the maximum value of the microwave oven used. Therefore, investigation with higher-power microwaves for short times was not possible.

CS, BS, and the density of alkali-activated mixture SRa irradiated with microwaves of different powers and durations, 28 d after moulding, are shown in the third row of Fig. 3(a–c), respectively.

From the contour plots, it can be seen that the highest CS and density of mixture SRa were achieved with microwave irradiation of 420 W for 20 s, whereas the highest BS was measured after irradiation at 560 W for 10–20 s. The sharp decrease in CS and BS began after the microwave power of 600 W, that is, samples irradiated with 700 W for different times showed large vertical cracks through the entire volume of the AAM (microwave irradiation is volumetric heating) owing to early water evaporation (all 2-dimensional cracks were vertical, i.e. perpendicular to the direction of moulding) or deterioration of the calcium-silicate-hydrate (CSH; which is the hydration product of portlandite [26] that can be present in ladle slags [27]) at “elevated” temperatures [28].

CS, BS, and the density of the alkali-activated mixture MKa irradiated with microwaves of different powers and durations, 28 d after moulding, are shown in the fourth row in Fig. 3(a–c), respectively.

The contour plots of the irradiated MKa, density, CS, and BS showed the highest values when irradiated with 700 W microwaves for a shorter time. However, the mixture MKa should be irradiated with microwaves of higher power for a shorter time to obtain the optimal irradiation parameters.

### 3.4. Compressive strength's time development of irradiated and not irradiated alkali-activated slurries

Fig. 4s a, b, c, and d show the 4-week time dependence of the CS of mixtures FAa, FAb, SRa and MKa irradiated with microwaves with a power of 700 W (P100, 100% of power of microwave) for 5–25 s (in 5 s

steps, the number of seconds of irradiation is labelled as tx, where x is the time of irradiation in seconds) compared to the non-irradiated (P0, 0% of the power of microwave) sample, respectively.

As shown in Fig. 4, besides solidification and drying after the initial alkali-activated chemical reaction, different chemical reactions took place a few weeks after moulding (which had positive and negative impacts on the development of CS), and the long-term limit of mechanical strengths may not be achieved after 1 month.

The alkali-activated mixture FAa (Fig. 4 a) overall shows the overall growth of CS with time. Although the CS of the non-irradiated sample was higher on day 7 than that of the irradiated samples, the majority of irradiated samples developed higher CS after a longer period. Only the samples irradiated for 5 and 15 s showed a decline in CS at 28 days, with a maximum on day 21 (CS should be followed until the limit is reached). All other samples had already reached the CS limit value of CS already in 21 days.

The CS of the irradiated alkali-activated mixture FAb (Fig. 4 b) showed a unique time dependence, that is, CS is concave with time, with a minimum value between 14 and 21 days, which is due to the positive/negative chemical reactions constantly taking place in the material, that is, mixture design is crucial and was reported in our previous work [21]. The weakest decline in CS occurred in the sample that was irradiated for only 5 s, while the CS of the sample that was not irradiated declined with time and probably reached the limit on day 28, as shown in Fig. 4 b.

In contrast, the CS of irradiated alkali-activated mixture SRa (Fig. 4 c) shows convex behaviour over 4 weeks with the maximal value 21 d after moulding (due to the formation of CSH, which is influenced by temperature [29] and moisture [30]), where the sample irradiated for 10 s showed the highest difference in CS values and reached the highest peak compared to all samples prepared from SRa (this experiment was repeated to exclude human error; however, as mentioned above, the material is “alive” and changes properties until the chemical reactions can occur [21]). The non-irradiated sample had the highest compressive strength on the 7th and 28th d and had slow growth over time after the

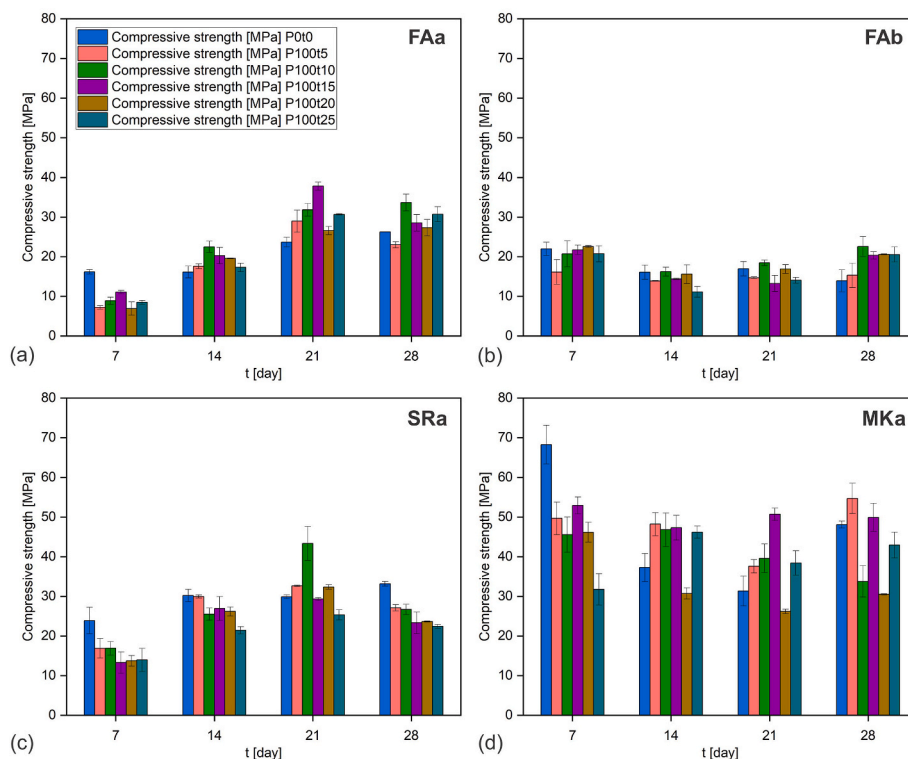


Fig. 4. Time dependence of CS for alkali-activated mixtures (a) FAa, (b) FAb, (c) SRa, and (d) MKa not irradiated (blue) and irradiated with microwaves of 700 W (100% power) for different time (red: 5 s, green: 10 s, purple: 15 s, brown: 20 s, and turquoise: 25 s). (For interpretation of the references to colour in this figure legend, the reader is referred to the Web version of this article.)

7th d, i.e., its CS was close to its limit value at 14 d (meaning that the majority of reactive ingredients in SR had already reacted in just a few days).

The time dependence of CS of alkali-activated mixture MKa is concave for the majority of samples except for the sample irradiated for 10 s (CS started to decrease after 14 d without being able to predict its future development) and 25 s (CS increases from the 7th to 14th d, after which the value decreases and shows concave behaviour to the 28th d without being able to predict its future behaviour). The CS of the sample irradiated for 15 s exhibited approximately constant time behaviour (fluctuations of approximately 50 MPa).

From all the experiments in this section, we can conclude that mixture design according to the amounts of elements in the amorphous phase is the most important step considering it influences further chemical development on the local scale with time regardless of the curing method used. The curing method can allow or hinder dissolution/diffusion and self-assembly (if there is only sufficient liquid for wetting, loss of liquid until the reaction can take place is not desirable; if there is enough liquid and sufficiently high energy transfer to the material, additional (non-desirable) elements can dissolve) and enhance/hinder the rate of material development/ageing.

### 3.5. Compressive strength's time development of optimally irradiated and not irradiated alkali-activated mixtures FAa and SRa with additional water

The short-term development of the CS of the non-irradiated and optimally irradiated slurries of mixtures FAa, FAd, FAe, and SRa, SRC, SRd is shown in Fig. 5, where the main focus is how additional water influences CS and how microwave irradiation influences CS when an excessive amount of water is present.

From Fig. 5, it is clear that the additional water decreases the CS values no matter the precursor or tested mixture or if the slurry was irradiated or not. In addition to excess water in general, as well as the potential hindering into the material, increasing non-uniformity of the temperature inside the material, FA requires more time to develop CS above 10 MPa, especially if there is more water in the mixture. In contrast, SR reached a CS of over 20 MPa in 7 d if there was not too much water added (SRd reached a CS value above 10 MPa in 28 d). The density increased with time until the maximum value for each mixture was reached. Irradiated samples' density and CS are generally slightly higher or comparable to their non-irradiated counterparts. This indicates that the addition of water did not hinder the penetration depth of microwaves in the prisms of dimensions  $(2 \times 2 \times 8) \text{ cm}^3$  (at least not significantly) while irradiating with the selected power and for the selected time. The temperature most likely did not increase to the point where

dehydration would be accelerated and cause damage to the material by a decrease in the dissolution/diffusion ability (amount of water decreased) and the creation of dehydration cracks.

### 3.6. X-ray diffraction analyses results of irradiated and not irradiated alkali-activated mixtures

Fig. 6 shows the Rietveld refinement results of the XRD patterns of the time development of non-irradiated and optimally irradiated slurries for mixtures FAa, FAd, FAe, and SRa, SRC, SRd; non-irradiated and irradiated slurries are labelled with 0 and 1, respectively (Rietveld refinement and XRD patterns of precursors and 156 d old non-irradiated and optimally irradiated optimally designed mixtures are presented in Supplementary Figs. S2 and S3; goodness of fit (GOF) for precursors FA, SR, and MK is 3.6, 6.5, and 8.3, respectively, and GOF's range for their alkali-activated counterparts is 3.6–4.4, 5.2–7.9, and 7.5–8.3, respectively; mineral cards with chemical formulas for solving XRD of precursors and AAMs are shown in Supplementary Table S1). When comparing precursors with their alkali-activated counterparts, there is a difference in the proportions of phases owing to the addition of an amorphous material (alkali) that is incorporated into the aluminosilicate network (ASN) or forms salts in the worst-case scenario (if there is an excess of alkali elements). The amounts of minerals that are present in the precursor in lower amounts can “disappear” because of the limit of XRD measurement (although they do not dissolve in alkali), and some new minerals can form (mostly salts).

However, there was no significant difference in the early stages of non-irradiated and irradiated AAMs in alkali-activated FA albite (containing Al, Si, O, and Na) and calcite formed as new minerals, and there was no difference between mixtures containing additional water (in the Rietveld refinement “error”). The amount of calcite increased in the FAa (and irradiated mixture FAe) samples after 156 d, which might also happen to the rest in a longer period. Furthermore, the amount of mineral mullite (containing Al, Si, O) increased, which could be chemically incorporated in ASN (crystallisation of usually mostly amorphous ASN) or present in ASN as a filler. The difference between the irradiated and non-irradiated samples was not obvious, regardless of the age of the samples. This indicates that the microwave power and irradiation time did not transfer enough energy to the material to break bonds in crystals (presented in Supplementary Fig. S3 on the long-term limit of optimally irradiated and non-irradiated FAa, SRa, and MKa).

In the case of alkali-activated SR mixtures, the amount of amorphous content increased owing to the addition of alkali used in the formation of amorphous ASN (this did not occur in the case of alkali-activated FA). One new mineral formed (brucite) equally in all samples (regardless of the amount of water and irradiation, non-irradiation), but more of them

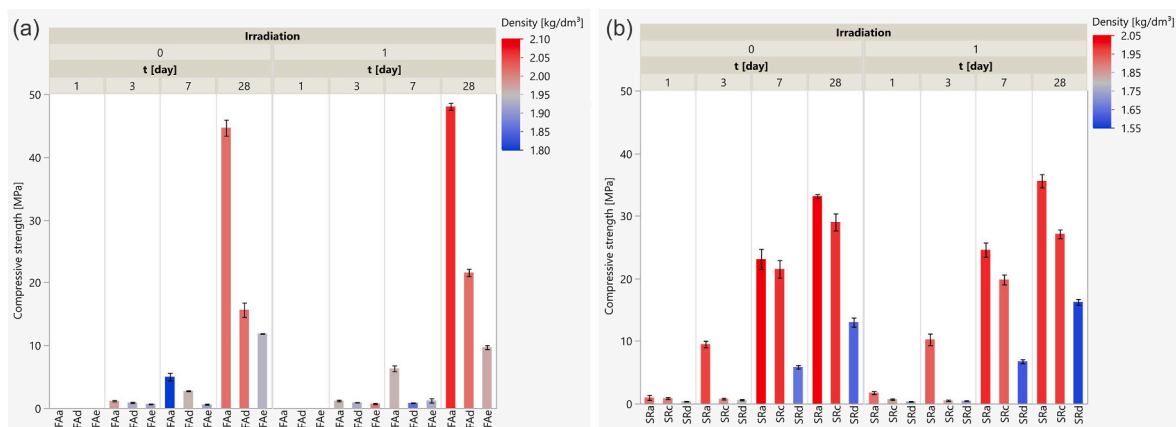
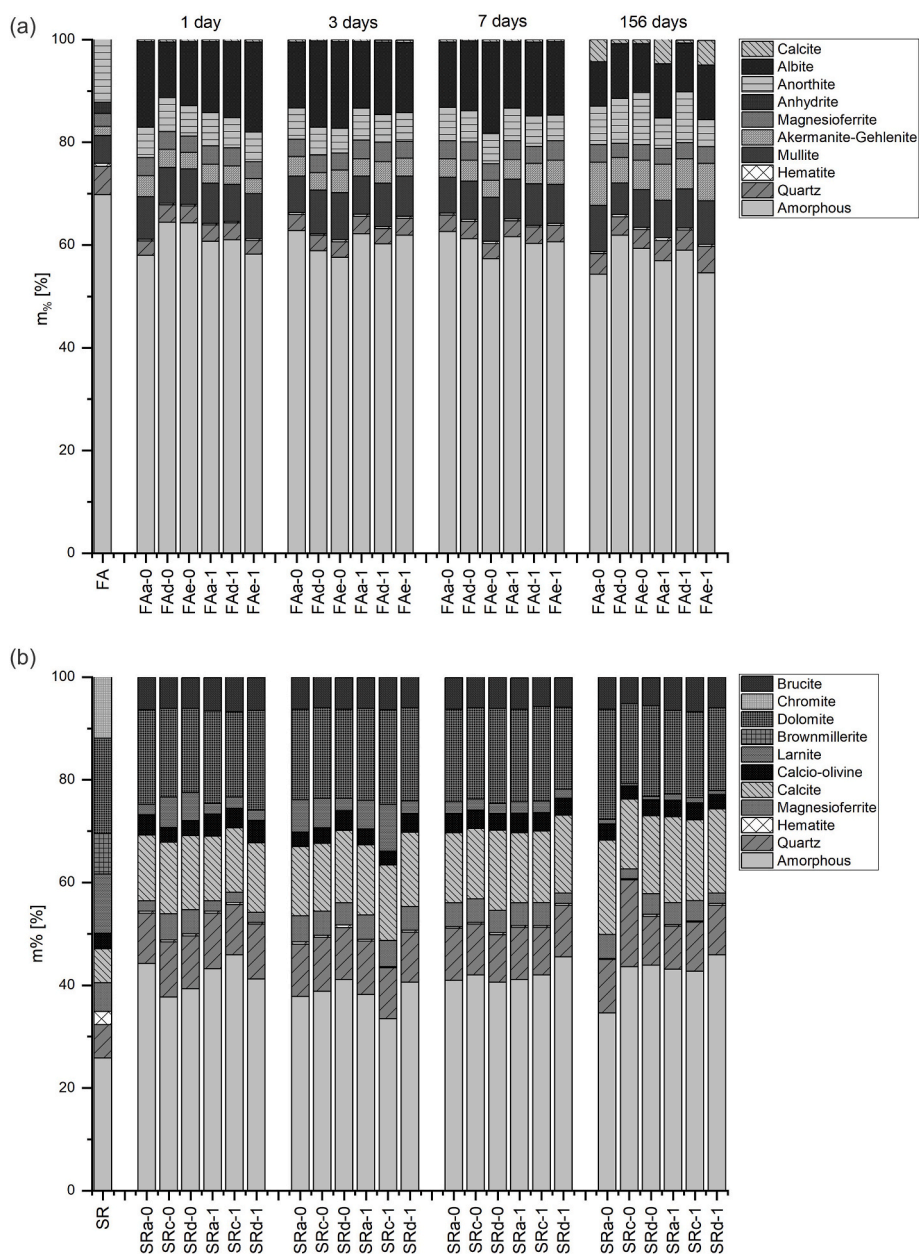


Fig. 5. Short-term time dependence of CS for not irradiated alkali-activated mixtures (0, left) and their optimally irradiated counterparts (1, right) of (a) FAa, FAd, FAe (irradiation for 15 s with 280 W), and (b) SRa, SRC and SRd (irradiation for 20 s with 420 W).



**Fig. 6.** XRD of FA and SR precursors used in the alkali-activated reaction with time development of not irradiated (0) and optimally irradiated (1) slurries of mixtures FAa, FAd, FAe, and SRa, SRC, SRd.

disappeared in the XRD patterns: brownmillerite and chromite completely (beyond the detection limit), and larnite partially. Larnite, as a low-calcium mineral, can transform into well-crystalline calcite in water and the presence of  $\text{CO}_2$  under just 2 bar and at  $24^\circ\text{C}$  [31], which most likely occurred during alkali activation of SR, considering the amount of calcite increased and the amount of larnite decreased. No significant difference was observed between the irradiated and non-irradiated alkali-activated SR slurries, as in FA-based AAMs, thereby indicating that microwave irradiation of chosen power and time did not (significantly enough) influence the crystal structure of any mineral (presented also in supplement in Fig. S3 on the long-term limit of optimally irradiated and non-irradiated SRa, and MKa).

### 3.7. FTIR analyses of irradiated and not irradiated alkali-activated mixtures

The FTIR results for the two precursors (FA and SR) and the time

development of their non-irradiated and optimally irradiated alkali-activated mixtures (FAa, FAd, FAe, and SRa, SRC, SRd) are shown in Figs. 7–9. FA shows the main band centred at  $999\text{ cm}^{-1}$  representing the T–O–Si (T = Si or Al) asymmetric stretch, as shown in Fig. 7. A wide, intense T–O bond asymmetric stretching vibration appears in the area between  $1250$  and  $850\text{ cm}^{-1}$  where quartz, mullite, and the vitreous phase of the ash overlap. The bands at  $775$  and  $794\text{ cm}^{-1}$  correspond to the presence of crystalline quartz, whereas the main Si–O stretching located at higher wavenumbers (e.g. at  $1085\text{ cm}^{-1}$  [32]) overlapped. Similarly, the main band at approximately  $1100\text{ cm}^{-1}$  of the mullite spectrum was barely observed owing to the overlapping. The bands at lower wavenumbers ( $676$ ,  $592\text{ cm}^{-1}$ ) may correspond to quartz and/or mullite. Unfortunately, unique vibrations that do not interfere with other silicate minerals are distinctly observed in the infrared spectrum [33].

The SR band at approximately  $987\text{ cm}^{-1}$  representing the T–O–Si (T = Si or Al) asymmetric stretch is shown in Fig. 7. A small peak at  $3694$

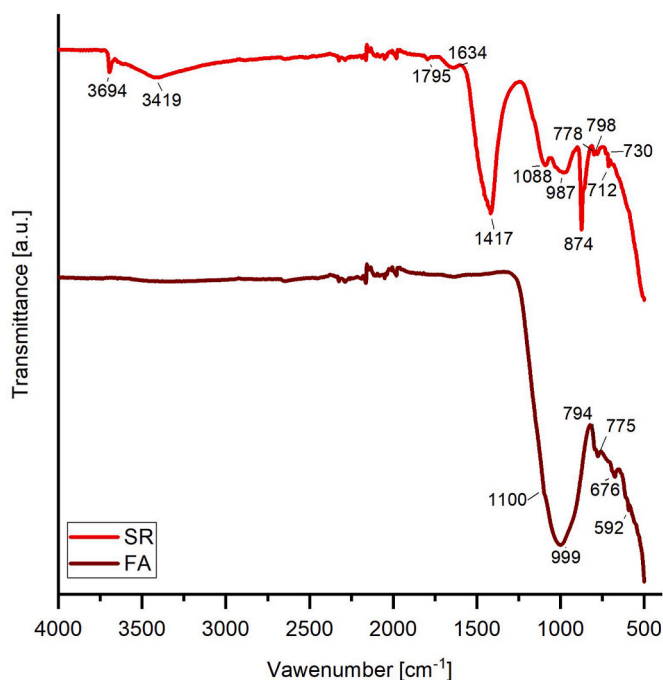


Fig. 7. FTIR spectra of precursors used for alkali activation, FA and SR.

$\text{cm}^{-1}$  belonged to brucite, and an extended band at  $3419 \text{ cm}^{-1}$  can be attributed to the stretching vibration bands of the hydroxyl groups [34, 35]. The bands at  $712$ ,  $874$ ,  $1088$ , and  $1795 \text{ cm}^{-1}$  belong to calcite [36, 37], whereas the most intense band at  $1417 \text{ cm}^{-1}$  overlaps both calcite and dolomite. However, the bands for calcite and dolomite partially overlapping [38,39]. The weak doublets at  $778$  and  $798 \text{ cm}^{-1}$  correspond to quartz. Additionally, the band at  $1088$  may be attributed to quartz [40]. The proportion of crystallites present in smaller amounts, according to XRD, cannot be observed in the FTIR spectrum. The difference in the bands belongs to the T–O–Si (T = Si or Al) asymmetric stretch, which is attributed to the different amorphous contents of the precursors [41].

In addition to FA having over twice as much of all potentially useful amorphous elements (Table 3, mass percentage of all useful elements) as the SR precursor, it is clear from the FTIR measurement (Fig. 7) that FA contains a higher amount of useful building blocks (T–O–Si, where T = Si or Al) in the ASN, as has a stronger and wider peak at  $999 \text{ cm}^{-1}$ , making FA a more reactive precursor than SR for alkali activation.

The main band formed during the alkali activation of FA was assigned to dissolved species liberated from FA by dissolution into the alkaline activating solution [42]. After the alkali activation of FA, similar locations of absorption bands were observed in the first 7 d (the middle of the peak at approximately  $930 \text{ cm}^{-1}$ ), regardless of whether microwaves were used (Fig. 8). The wide absorption band at  $3310$  and narrower band at  $1647 \text{ cm}^{-1}$  correspond to the vibrations of hydroxyl groups [43]. The barely visible band at  $1100 \text{ cm}^{-1}$  can be attributed to the mullite present in the FA that did not dissolve during alkali activation [44–47]. After 7 d, bands due to chemically bound water within the hydration products at approximately  $3310$  and  $1647 \text{ cm}^{-1}$  decreased within the samples prepared using microwaves. However, some water remained in the samples. The main band centred at  $930 \text{ cm}^{-1}$  was assigned to the T–O–Si (T = Si or Al) asymmetric stretch of  $\text{TO}_4$  tetrahedra, which was typical of amorphous aluminosilicate glass [33]. However, after alkali activation, double bands were seen in the FA samples associated with terminal Si–O<sup>-</sup> bonds and –Si–O (Si) bridge bonds, and both were located in the  $1100$ – $900 \text{ cm}^{-1}$  range where the bridging vibration occurred at higher wavenumbers [48,49]. The band characteristic of 6-membered silicoxygen rings occurred at  $617 \text{ cm}^{-1}$

and the appearance of additional bands in the spectra resulted from the lowering of the hexagonal symmetry of the rings. However, this band was observed after 156 d and not 1, 3, or 7 d (Fig. 8).

The asymmetric stretching vibrations of the Si–O–T band are sensitive to the ASN structure, where other factors such as the length and angle of Si–O–T bonds and next-nearest neighbour effects decrease the molecular vibrational force constant and shift the asymmetric stretch to lower wavenumbers [50,51].

When the concentration of the alkali solution increased, the peak positions for Si–O–Si and Si–O–Al asymmetric stretching shifted slightly to lower wavenumbers [46]. However, the same amounts of NaOH and Na-water glass solution were present in FAa, FAd, and FAe, and the only difference between these samples was the amount of water (FAa < FAd < FAe), and the positions of the bands (comprising two peaks) were similar up to 7 d. Shifting to lower wavenumbers indicates depolymerisation of the original silicate and/or aluminosilicate structures in the FA mixtures. Al causes depolymerisation of the structure owing to the widening of the absorption band at  $1300$ – $850 \text{ cm}^{-1}$ . The increased content results in a band shift to a lower wavenumber due to the partial substitution of Si–O–Si by Si–O–Al bonds [52]. However, because of the various amounts of water in the samples, the ratios of  $\text{H}_2\text{O}/\text{SiO}_2$  and  $\text{OH}^-/\text{SiO}_2$  significantly implemented the “molecular” or “polymeric” species present in the reaction mix composition and the rate at which these species were incorporated into the three-dimensional structure [44]. After 156 d, one band shifted to higher wavenumbers considering the silica content of the product increased with reaction time [46]. Moreover, the shifts were positioned at the same wavenumber ( $956 \text{ cm}^{-1}$ ) for all irradiated and non-irradiated samples, which indicated the formation of similar ASN structures in all samples.

Figure 8(b) shows the results of the FTIR analyses for alkali-activated SR samples with the same amount of Na-water glass and different amounts of water (SRa < SRc < SRd). After alkali activation of SR, bands at approximately  $3340$  and  $1646 \text{ cm}^{-1}$  were related to O–H bending and  $\text{H}_2\text{O}$  stretching in the absorbed water [53]. The band at  $1417 \text{ cm}^{-1}$  was assigned to the asymmetric stretching vibrations of C–O–C bonds in  $\text{CO}_3^{2-}$  [54], and the weak shoulder at approximately  $872 \text{ cm}^{-1}$  owing to out-of-plane bending. After 1 d of curing, alkali-activated SR samples showed bands in the range of  $958$ – $964 \text{ cm}^{-1}$  for irradiated and  $958$ – $968 \text{ cm}^{-1}$  for non-irradiated samples. However, in all samples, except for the irradiated sample SRd, shifts to lower wavenumbers were observed after 7 d of curing. The increased wavenumber of the asymmetric stretching band of the Si–O–T bonds was ascribed to the degree of polymerisation [43]. The shifts to lower wavenumbers can be attributed to the availability of Ca from the slag precursor [55]. In addition, by incorporating Al released from the SR to the ASN (or due to the decrease of network connectivity), the Si:Al ratio decreased, which shifted the vibration band to a lower wavenumber [56,57]. The observed shift of the Si–O–Si (Al) band to lower wavenumbers can be attributed to the change in the ASN composition, where the substitution of  $\text{Ca}^{2+}$  for  $\text{Na}^+$  in the ASN decreased the bridging O atom in the Si–O tetrahedral and the degree of polymerisation of the hydration products [58]. However, after monitoring for longer curing times, the degree of polymerisation of the binder may increase, and more Si from the slag particles can be incorporated into the ASN [55], as observed after 156 d of curing sample SR while shifting to higher wavenumbers. The irradiated mixture SRd was the only sample wherein the wavenumbers shifted to a higher value after 7 d and not 156 d of curing. However, the non-irradiated mixture SRd shifted to lower wavenumbers after 156 d. The SRd sample contained the highest amount of water, and its ASN reorganisation process had not yet ended.

Fig. 9 shows the shifts in the minima of the ASN peak for mixtures of FA (a) and SR (b). In the case of FA-based AAMs, the behaviour of these shifts showed no significant difference if there was more/less water or if the material was irradiated. Conversely, SR-based AAMs showed comparable behaviour, except for SRd, which contained the largest amount of water. The non-irradiated mixture SRd “FTIR-chemically” caught the

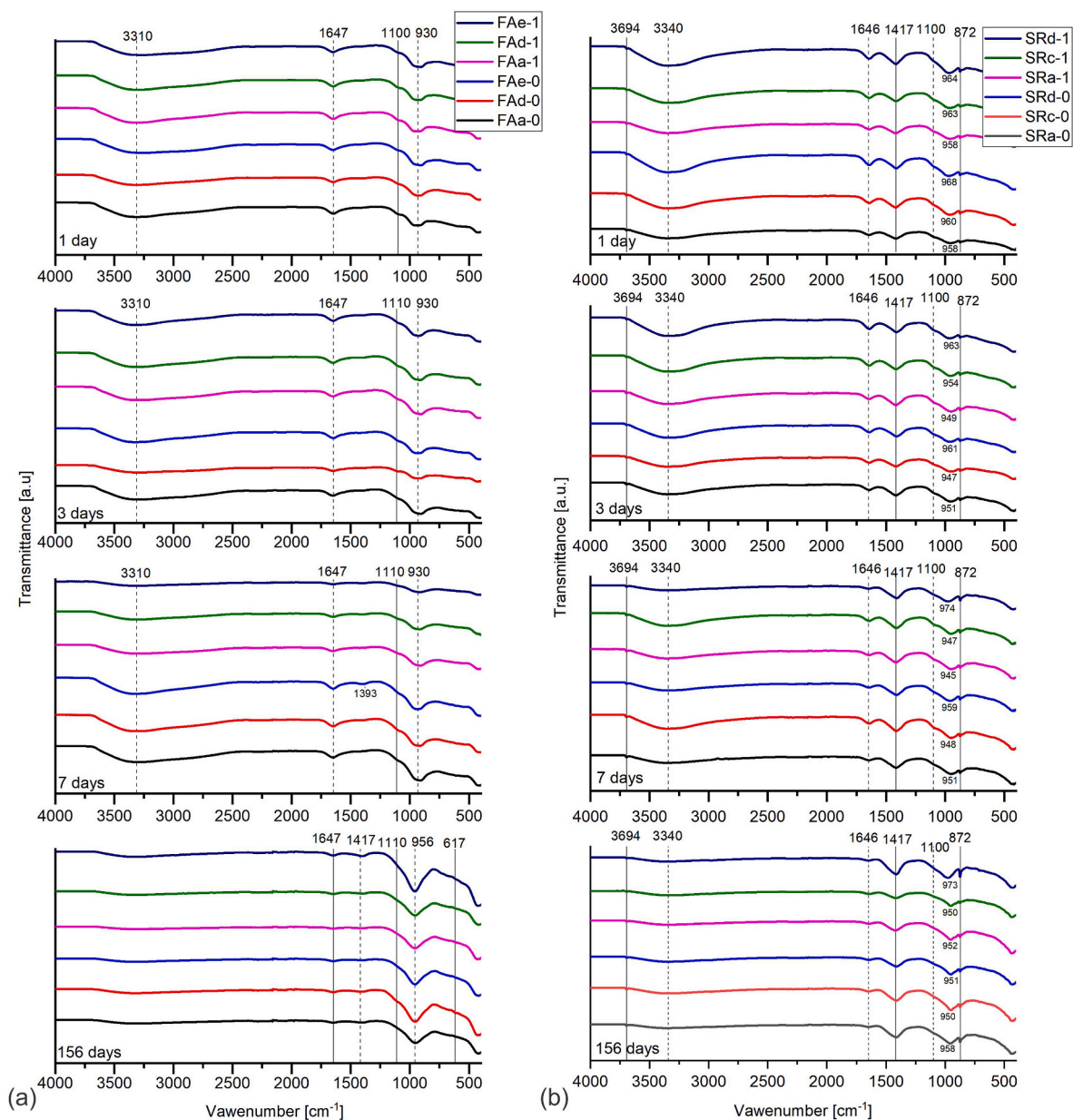


Fig. 8. FTIR spectra of alkali-activated irradiated (1) and non-irradiated (0) samples of (a) FA and (b) SR mixtures.

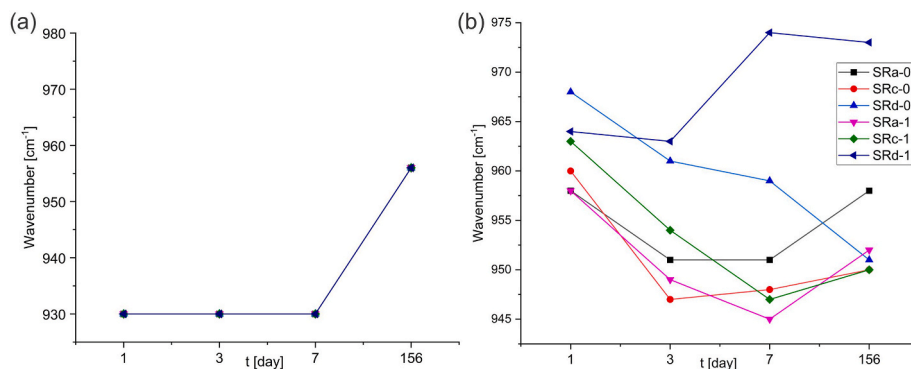


Fig. 9. Shifts of FTIR minima (peak assigned to ASN) of alkali-activated irradiated (1) and non-irradiated (0) samples of (a) FA and (b) SR mixtures.

ASN composition with other samples in 156 d, while the irradiated SRD sample required more time or its behaviour is different owing to the microwave irradiation. The correct amount of water and energy transfer from microwaves to the slurry in its early stages enhanced the dissolution of elements (amorphous Si and Al) and influenced the time development of ASN, but not at the same rate as for non-irradiated samples.

#### 4. Conclusions

The compressive and bending strengths of AAMs showed a time dependence on the age of the AAM, which was heavily influenced by the dose of microwave irradiation (duration of irradiation and power of microwaves), which in turn was heavily influenced by the material used as a precursor. Therefore, conclusions from experiments on one precursor cannot be drawn from another precursor. Every single mixture (precursor mixed with liquid alkali) was evaluated-mapped on P/t of microwave irradiation before optimising the amount of water at P/t that provides maximal mechanical strength values to keep enough water in the slurry for the diffusion of dissolved elements and their rearrangement in the ASN during alkali activation after irradiation when part of the water evaporates due to higher temperatures (that helped with dissolution).

Regardless of the precursor or mixture, an additional amount of water decreased the compressive strength and density. Irradiating with optimal microwave power and optimal time for the chosen mixture and precursor usually results in a slightly higher compressive strength and density compared to non-irradiated samples.

XRD and FTIR did not show obvious changes between the irradiated and non-irradiated samples, that is, the irradiation only enhances the dissolution of the amorphous content if the material receives sufficient microwave energy (not so much to significantly affect dehydration). Moreover, the addition of water did not noticeably influence the mineralogy or the ASN. ASN and its properties, therefore, depend primarily on the chemistry of the mixture (precursor and alkali) and the age of the AAM (chemical reactions also occur after curing).

However, to obtain more detailed information about the structural changes during the irradiation process and the influence of power and time of irradiation on alkali activation and ASN formation, NMR analysis will be performed in future studies.

#### Author contributions

Conceptualisation, B.H., M.P., and V.D.; data curation, B.H., M.P. formal analysis, B.H., M.P.; investigation, B.H., M.P.; methodology, B.H., M.P., and V.D.; validation, B.H., M.P.; visualisation, B.H., M.P.; writing – original draft, B.H.; writing – review and editing, B.H., M.P., and V.D.

#### Funding

This work was part of the ARRS project of Dr. Barbara Horvat and was financially supported by the Slovenian Research Agency under Grant no. J2-3035. The involvement of Dr. Majda Pavlin was financially supported by the postdoc project of Dr. Majda Pavlin, which is financially supported by the Slovenian Research Agency under Grant no. Z2-3199. Dr. Vilma Ducman was supported by the Slovenian Research Agency Program Group P2-0273.

#### Declaration of competing interest

The authors declare that they have no known competing financial interests or personal relationships that could have appeared to influence the work reported in this paper.

#### Acknowledgements

The Metrology Institute of the Republic of Slovenia is acknowledged for its use of XRF.

#### Appendix A. Supplementary data

Supplementary data to this article can be found online at <https://doi.org/10.1016/j.ceramint.2022.12.133>.

#### References

- [1] J. Davidovits, Geopolymers - inorganic polymeric new materials, *J. Therm. Anal.* 37 (1991) 163316–163356.
- [2] J. Provis, Alkali activated materials: state-of-the-art report, in: RILEM TC 224-AAM, Springer, New York, 2013, ISBN 978-94-007-7671-5.
- [3] P. Duxson, J.L. Provis, G.C. Lukey, S.W. Mallicoate, W.M. Kriven, J.S.J. van Deventer, Understanding the relationship between geopolymer composition, microstructure and mechanical properties, *Colloids Surf. A Physicochem. Eng. Asp.* 269 (2005) 47–58, <https://doi.org/10.1016/j.colsurfa.2005.06.060>.
- [4] B. Horvat, A.S. Pavlin, V. Ducman, Foundry wastes as potential precursor in alkali activation technology, in: Proceedings of the Technologies & Business Models for Circular Economy, Univerzitetna založba Univerze v Mariboru/University of Maribor Press, 2019.
- [5] F. Škvárka, Alkali Activated Material - Geopolymer, vol. 16, 2007.
- [6] Shell Mold Casting, Available online: [https://thelibraryofmanufacturing.com/hell\\_mold\\_casting.html](https://thelibraryofmanufacturing.com/hell_mold_casting.html). (Accessed 14 November 2019).
- [7] A. Borrell, M.D. Salvador, Advanced ceramic materials sintered by microwave technology, in: M. Liu (Ed.), Sintering Technology - Method and Application, InTech, 2018, ISBN 978-1-78984-281-4.
- [8] Microwave heating - physical basics in the molecule, Available online: <https://www.pueschner.com/en/microwave-technology/physical-basics>. (Accessed 6 October 2022).
- [9] C. Antonio, R. Deam, A. Taube, A review of the variable frequency microwave technology in material processing, *J. Microw. Power Electromagn. Energy* 38 (2003) 75–87, <https://doi.org/10.1080/08327823.2003.11688488>.
- [10] Soltysiak, M.; Celuch, M.; Erie, U. Measured and Simulated Frequency Spectra of the Household Microwave Oven. vol. 4.
- [11] Park, C.-W.; Park, J.S.; Kim, H. Synthesis of Coal Bottom Ash (CBA)-Based Geopolymer with Microwave Energy Appended to Conventional Dry-Oven Curing Process. vol. 1.
- [12] S. Hong, H. Kim, Rapid Compressive Strength Achievement of Coal Bottom Ash Based Geopolymer by Employing Microwave Energy, vol. 4, 2018.
- [13] S. Hong, H. Kim, Robust synthesis of coal bottom ash-based geopolymers using additional microwave heating and curing for high compressive strength properties, *Kor. J. Chem. Eng.* 36 (2019) 1164–1171, <https://doi.org/10.1007/s11814-019-0286-y>.
- [14] S. Hong, H. Kim, Effects of microwave energy on fast compressive strength development of coal bottom ash-based geopolymers, *Sci. Rep.* 9 (2019), <https://doi.org/10.1038/s41598-019-52160-2>.
- [15] M.M. Al Bakri Abdullah, M.F. Mohd Tahir, K. Hussin, M. Binhussain, J.J. Ekaputri, Effect of microwave curing to the compressive strength of fly ash based geopolymer mortar, *Mater. Sci. Forum* 841 (2016) 193–199, <https://doi.org/10.4028/www.scientific.net/MSF.841.193>.
- [16] S.K. Saxena, M. Kumar, N.B. Singh, Influence of alkali solutions on properties of pond fly ash-based geopolymer mortar cured under different conditions, *Adv. Cement Res.* 30 (2018) 1–7, <https://doi.org/10.1680/jadcr.17.00038>.
- [17] A. Graytee, J.G. Sanjayana, A. Nazari, Development of a high strength fly ash-based geopolymer in short time by using microwave curing, *Ceram. Int.* 44 (2018) 8216–8222, <https://doi.org/10.1016/j.ceramint.2018.02.001>.
- [18] S. Onutai, S. Jiemsirilers, P. Thavorniti, T. Kobayashi, Fast microwave syntheses of fly ash based porous geopolymers in the presence of high alkali concentration, *Ceram. Int.* 42 (2016) 9866–9874, <https://doi.org/10.1016/j.ceramint.2016.03.086>.
- [19] A. Kusiantoro, M.F. Nuruddin, N. Shafiq, S.A. Qazi, The effect of microwave incinerated rice husk ash on the compressive and bond strength of fly ash based geopolymer concrete, *Construct. Build. Mater.* 36 (2012) 695–703, <https://doi.org/10.1016/j.conbuildmat.2012.06.064>.
- [20] O.A. Panitsa, D. Kioupis, G. Kakali, Thermal and microwave synthesis of silica fume-based solid activator for the one-Part Geopolymerization of fly ash, *Environ. Sci. Pollut. Res.* 29 (2022) 59513–59523, <https://doi.org/10.1007/s11356-022-20081-9>.
- [21] B. Horvat, V. Ducman, Potential of Green Ceramics Waste for Alkali Activated Foams, vol. 30, 2019.
- [22] B. Horvat, V. Ducman, Influence of particle size on compressive strength of alkali activated refractory materials, *Materials* 13 (2020) 2227, <https://doi.org/10.3390/ma13102227>.
- [23] Y. Luo, K.M. Klima, H.J.H. Brouwers, Q. Yu, Effects of ladle slag on class F fly ash geopolymer: reaction mechanism and high temperature behavior, *Cement Concr. Compos.* 129 (2022), 104468, <https://doi.org/10.1016/j.cemconcomp.2022.104468>.

- [24] K.S. Rao, G. Chandra, P.V. Narasimha Rao, Study on penetration depth and its dependence on frequency, soil moisture, texture and temperature in the context of microwave remote sensing, *J Indian Soc Remote Sens* 16 (1988) 7–19, <https://doi.org/10.1007/BF03014300>.
- [25] Spencer, P. Technology Brief 3: Microwave Ovens. vol. 2.
- [26] X. Guo, H. Shi, L. Chen, W.A. Dick, Alkali-activated complex binders from class C fly ash and Ca-containing admixtures, *J. Hazard Mater.* 173 (2010) 480–486, <https://doi.org/10.1016/j.jhazmat.2009.08.110>.
- [27] D. Aponte, O. Soto Martín, S. Valls del Barrio, M. Barra Bizinotto, Ladle steel slag in activated systems for construction use, *Minerals* 10 (2020) 687, <https://doi.org/10.3390/min10080687>.
- [28] M.A. Tantawy, Effect of high temperatures on the microstructure of cement paste, *Inside MS* (2017) 33–48, <https://doi.org/10.4236/msce.2017.511004>, 05.
- [29] E. Tajuelo Rodriguez, K. Garbev, D. Merz, L. Black, I.G. Richardson, Thermal stability of C-S-H phases and applicability of richardson and groves' and richardson C-(A)-S-H(I) models to synthetic C-S-H, *Cement Concr. Res.* 93 (2017) 45–56, <https://doi.org/10.1016/j.cemconres.2016.12.005>.
- [30] C. Alonso, L. Fernandez, Dehydration and rehydration processes of cement paste exposed to high temperature environments, *J. Mater. Sci.* 39 (2004) 3015–3024, <https://doi.org/10.1023/B:JMISC.0000025827.65956.18>.
- [31] D. Wang, Y. Fang, Y. Zhang, J. Chang, Changes in mineral composition, growth of calcite crystal, and promotion of physico-chemical properties induced by carbonation of  $\beta$ -C<sub>2</sub>S, *J. CO<sub>2</sub> Util.* 34 (2019) 149–162, <https://doi.org/10.1016/j.jcou.2019.06.005>.
- [32] Z. Zhang, H. Wang, J.L. Provis, Quantitative study of the reactivity of fly ash in geopolymerization by FTIR, *Journal of Sustainable Cement-Based Materials* 1 (2012) 154–166.
- [33] R.K. Vempati, A. Rao, T.R. Hess, D.L. Cocke, H.V. Lauer Jr., Fractionation and characterization of Texas lignite class 'F' fly ash by XRD, TGA, FTIR, and SFM, *Cement Concr. Res.* 24 (1994) 1153–1164.
- [34] F. Wypych, W.H. Schreiner, N. Mattoso, D.H. Mosca, R. Marangoni, C.A. Bento, S. da, Covalent grafting of phenylphosphonate groups onto layered silica derived from in situ-leached chrysotile fibers, *J. Mater. Chem.* 13 (2003) 304–307.
- [35] X. Wang, H. Pang, W. Chen, Y. Lin, G. Ning, Nanoengineering core/shell structured brucite@ polyphosphate@ amine hybrid system for enhanced flame retardant properties, *Polym. Degrad. Stabil.* 98 (2013) 2609–2616.
- [36] J.D. Rodriguez-Blanco, S. Shaw, L.G. Benning, The kinetics and mechanisms of amorphous calcium carbonate (ACC) crystallization to calcite, via vaterite, *Nanoscale* 3 (2011) 265–271.
- [37] D. Chakrabarty, S. Mahapatra, Aragonite crystals with unconventional morphologies, *J. Mater. Chem.* 9 (1999) 2953–2957.
- [38] V.J. Bruckman, K. Wriessnig, Improved soil carbonate determination by FT-IR and X-ray analysis, *Environ. Chem. Lett.* 11 (2013) 65–70, <https://doi.org/10.1007/s10311-012-0380-4>.
- [39] B. Xu, K.M. Poduska, Linking crystal structure with temperature-sensitive vibrational modes in calcium carbonate minerals, *Phys. Chem. Chem. Phys.* 16 (2014) 17634–17639.
- [40] R. Shahack-Gross, O. Bar-Yosef, S. Weiner, Black-coloured bones in hayonim cave, Israel: differentiating between burning and oxide staining, *J. Archaeol. Sci.* 24 (1997) 439–446, <https://doi.org/10.1006/jasc.1996.0128>.
- [41] X. Gao, Q.L. Yu, H.J.H. Brouwers, Reaction kinetics, gel character and strength of ambient temperature cured alkali activated slag–fly ash blends, *Construct. Build. Mater.* 80 (2015) 105–115.
- [42] C.A. Rees, J.L. Provis, G.C. Lukey, J.S.J. van Deventer, Attenuated total reflectance fourier transform infrared analysis of fly ash geopolymer gel aging, *Langmuir* 23 (2007) 8170–8179.
- [43] P. Yu, R.J. Kirkpatrick, B. Poe, P.F. McMillan, X. Cong, Structure of calcium silicate hydrate (C-S-H): near-, mid-, and far-infrared spectroscopy, *J. Am. Ceram. Soc.* 82 (1999) 742–748, <https://doi.org/10.1111/j.1151-2916.1999.tb01826.x>.
- [44] M. Criado, A. Fernández-Jiménez, A. Palomo, Alkali activation of fly ash: effect of the SiO<sub>2</sub>/Na<sub>2</sub>O ratio: Part I: FTIR study, *Microporous Mesoporous Mater.* 106 (2007) 180–191.
- [45] R. Gören, B. Ersoy, C. Özgür, T. Alp, Colloidal stability–slip casting behavior relationship in slurry of mullite synthesized by the USP method, *Ceram. Int.* 38 (2012) 679–685, <https://doi.org/10.1016/j.ceramint.2011.07.056>.
- [46] A. Fernández-Jiménez, A. Palomo, Mid-infrared spectroscopic studies of alkali-activated fly ash structure, *Microporous Mesoporous Mater.* 86 (2005) 207–214, <https://doi.org/10.1016/j.micromeso.2005.05.057>.
- [47] J. Temuujin, K. Okada, K.J.D. MacKenzie, Effect of mechanochemical treatment on the crystallization behaviour of diphasic mullite gel, *Ceram. Int.* 6 (1999).
- [48] M. Sitarz, M. Handke, W. Mozgawa, E. Galuskin, I. Galuskina, The non-ring cations influence on silicoxygen ring vibrations, *J. Mol. Struct.* 555 (2000) 357–362.
- [49] M. Sitarz, W. Mozgawa, M. Handke, Vibrational spectra of complex ring silicate anions—method of recognition, *J. Mol. Struct.* 404 (1997) 193–197.
- [50] P. Innocenzi, Infrared spectroscopy of sol–gel derived silica-based films: a spectromicrostructure overview, *J. Non-Cryst. Solids* 316 (2003) 309–319.
- [51] A. Agarwal, M. Tomozawa, Correlation of silica glass properties with the infrared spectra, *J. Non-Cryst. Solids* 209 (1997) 166–174, [https://doi.org/10.1016/S0022-3093\(96\)00542-X](https://doi.org/10.1016/S0022-3093(96)00542-X).
- [52] E. Kapeluszná, L. Kotwica, A. Różycka, L. Golek, Incorporation of Al in CASH gels with various Ca/Si and Al/Si ratio: microstructural and structural characteristics with DTA/TG, XRD, FTIR and TEM analysis, *Construct. Build. Mater.* 155 (2017) 643–653.
- [53] J.C. Swanepoel, C.A. Strydom, Utilisation of fly ash in a geopolymeric material, *Appl. Geochem.* 17 (2002) 1143–1148.
- [54] M. Catauro, A. D'Angelo, S. Piccollella, C. Leonelli, G. Dal Poggetto, Influence of the addition of waste glass and microbiological performance of metakaolin-based geopolymers cement, *Macromol. Symp.* 404 (2022), 2100290, <https://doi.org/10.1002/masy.202100290>.
- [55] S.A. Bernal, J.L. Provis, V. Rose, R. Mejía de Gutierrez, Evolution of binder structure in sodium silicate-activated slag–metakaolin blends, *Cement Concr. Compos.* 33 (2011) 46–54, <https://doi.org/10.1016/j.cemconcomp.2010.09.004>.
- [56] Z. Zhang, Y. Zhu, H. Zhu, Y. Zhang, J.L. Provis, H. Wang, Effect of drying procedures on pore structure and phase evolution of alkali-activated cements, *Cement Concr. Compos.* 96 (2019) 194–203, <https://doi.org/10.1016/j.cemconcomp.2018.12.003>.
- [57] C.A. Rees, J.L. Provis, G.C. Lukey, J.S. van Deventer, In situ ATR-FTIR study of the early stages of fly ash geopolymer gel formation, *Langmuir* 23 (2007) 9076–9082, <https://doi.org/10.1021/la701185g>.
- [58] F. Puertas, A. Fernández-Jiménez, M.T. Blanco-Varela, Pore solution in alkali-activated slag cement pastes. Relation to the composition and structure of calcium silicate hydrate, *Cement Concr. Res.* 34 (2004) 139–148, [https://doi.org/10.1016/S0008-8846\(03\)00254-0](https://doi.org/10.1016/S0008-8846(03)00254-0).